CHAPTER 4

MULTISCALE SIMULATION USING NONSTANDARD WAVELET TRANSFORM

****

In the chapter 3, finite element equations are transformed using discrete wavelets. The standard form of the matrix for wave propagation and other problems are solved. To further reduce computational costs, nonstandard (NS) wavelet operator is employed for the multiresolution analysis. The remarkable feature of the nonstandard form is the uncoupling among scales. The wave propagation in the simple plate structures is discussed in the previous chapter. The modeling of waveguides with plate structures with damage is considered in this chapter. NS wavelet based multi-scale operator developed by using finite element discretization is used to represent waves. The proposed masking eliminates the requirement of a very large number of nodes in finite element method necessary for the propagation of such waves. In this work, the results of wavelet based dynamic adaptive grid selection technique are compared with the standard finite element method.

In this chapter, necessary background on the nonstandard wavelet operator is discussed in section 4.1. The mathematical background and algorithm for utilization of NS operator for multiscale method are presented in Section 4.2. This is highly advantageous and computationally efficient because the computation requires only few vector multiplications. Numerical examples in Section 4.3 show the applicability of the proposed technique to various plate structures.

4.1 Introduction

Material softening leading to nonlinearity in stress-strain relations prior to crack initiations is a common phenomenon in the structures which are subjected to cyclic loadings. The material nonlinearity of the structure generates higher harmonics when fundamental Rayleigh surface waves or Lamb waves are used in monitoring the health. Measurements of higher harmonics, particularly second harmonics are often used by the researchers in their experiments for early detection of structure failure (Deng (1999, 2003), Korobov and Izosimova (2006), Pruell *et al.* (2009), Li *et al.* (2012)).

Beylkin and Keiser (1997) used wavelet expansion for adaptively updating numerical solution of nonlinear PDEs, which exhibit both smooth and shock-like behaviour. The research in PDE simulations (Qian and Weiss (1993 A) and Amaratunga and Williams (1994)) was limited to simple domain and boundary conditions. Dahmen *et al.* (1999) proposed method to generate a sparse matrix by using wavelets and suggested accurately computing necessary coefficients and ignoring coefficients which create very little effects on the accuracy of the solution. Due to continuous wave propagation in the large domain, the location of necessary coefficients of the matrix will change continuously, therefore this cannot be an effective method. This method decouples coarse solution and refinement process for some problems but it is applicable to a specific problem and it could not be applied in wave propagation problems. Moreover, there is no need to use non-uniform grid proposed by them for such types of problems because wave propagation process is continuous and uniform. Nonlinear 1D advection-diffusion-reaction equation has been used by Alves *et al.* (2002) to compare wavelet based adaptive linear differencing schemes such as first order upwind, second order upwind, downward differencing, third order quadratic upwind and central difference schemes. Two-

dimensional wavelet optimized finite difference method has been used by Jameson and Miyama (2000) to solve oceanography problem. Yousefi *et al.* (2010) has used local Lagrange interpolation for spatial derivative and wavelets for the adaptive grid to solve the problem of elastic wave propagation in plates. Pei *et al.* (2009) has solved 2D first order stress-velocity acoustic wave equation by using wavelet optimized adaptive grid finite difference method. In the literature, some researchers have used wavelets as basis function to solve PDEs but most researchers have applied the wavelet based adaptive technique in finite difference schemes. These papers have presented the adaptive method for propagation of a single wave but there is a need of different algorithm for more than one waves propagating with different velocities. Generation of higher harmonics due to material nonlinearity is not addressed in these papers.

Two observations can be made while solving some PDEs using the wavelet bases:

(i) In theoretical terms, most of the available wavelet methods have stable Riesz basis and better condition number than FEM or FDM. (ii) But in practical applications wavelet methods are not yet ready to compete with the traditional FEM approach. One important reason is while the FEM can always produce a sparse matrix with more regular sparsity patterns, use of wavelet bases doesn't produce such sparse matrices. But the combination of wavelets with other methods FDM, FEM, and recently SEM (Mitra and Gopalakrishnan (2006)) show good results. Here we have used FEM discretization to derive a sparse matrix, as the FEM remains the most versatile tool to solve PDEs. First, the stiffness matrix for Lamb wave problem is formed then DWT based on pyramidal algorithms is used to modify the matrix. The method offers a purely algebraic way of using wavelets for wave propagation problems. This discrete approach also improves condition number of the matrix i.e. it can be used for preconditioning purpose also.

Beylkin *et al.* (1991) proposed a class of numerical algorithms for fast, effective computation of the linear operators on arbitrary vectors. This is known as theory of NS wavelet decomposition of linear operators. The NS form has been presented to offer a sparse representation for a wide class of operators by expanding the linear operator (matrix) and the input vector in a discrete wavelet basis. These algorithms may be applied to all operators whose integral (or distributional) kernels are smooth away from their main diagonals.

For the current problem, the major challenge is to develop dynamic adaptive grid over a long distance in a structure to propagate many short pulses which may contain higher harmonics also. The thesis is presenting wavelet based NS operator to improve finite element simulation of waves moving at different speeds in a large structure. We have used standard operator in previous chapter 3 but in the present analysis, we use nonstandard operator because it is more efficient than standard operator (Beylkin (1992)). This will not only be useful to the structural health monitoring but it can be used where waves with higher harmonics move at different group velocities. A simple description of the NS operator along with necessary algorithm and mathematical comments are provided to remove an implementation headache associated with adaptive grid techniques. The algorithm is applied to 2D plane strain problem, but it is general and independent of domain dimension.

4.2 Mathematical Formulation

4.2.1 Nonstandard (NS) wavelet transform

In this section, multiresolution analysis of nonstandard wavelet operators is presented (Beylkin *et al.* (1991), Gines *et al.* (1998)).

Let us consider a multiresolution analysis of $L^2(\mathbb{R})$. The operator T denoted the following form:

$$T : L^2(\mathbb{R}) \to L^2(\mathbb{R}) \tag{4.1}$$

The aim is to represent the operator T in the wavelet spaces. The subspaces W_j is defined as orthogonal complements of V_j in V_{j+1}

$$V_{j+1} = V_j \oplus W_j \tag{4.2}$$

If the number of scales is finite, we consider $j = n$ as a finest scale then $V_n \supset \cdots \supset V_2 \supset V_1 \supset V_0$, and $V_n \subset L^2(\mathbb{R})$.The subspace V_n has a finite dimension. The projection of the operator in the approximation subspace V_j, $j \in Z$ where Z is set of integers, can be written as:

$$P_j : L^2(\mathbb{R}) \to V_j \tag{4.3}$$

and expanding operator T in a "telescopic" or multiresolution form, we obtain

$$T = \sum_{j=\infty}^{0} \left(Q_j T Q_j + Q_j T P_j + P_j T Q_j \right) + P_0 T P_0 \tag{4.4}$$

where

$$Q_j : L^2(\mathbb{R}) \to W_j \tag{4.5}$$

If the scale $j=n$ is the finest scale, then

$$T_n = \sum_{j=n-1}^{0} \left(Q_j T Q_j + Q_j T P_j + P_j T Q_j \right) + P_0 T P_0, \tag{4.6}$$

where $T \sim T_n = P_n T P_n$ is a discretization of T on the finest scale. In the above equation

$Q_j TP_j$ and $P_j TQ_j$ represent interrelationship effects of subspaces V_j and W_j.

The NS form proposed by Bleykin (1992) is a representation of an operator *T* as a chain of tripletes as follows:

$$T = \left\{ \left\{ A_j, B_j, \Gamma_j \right\}_{\infty \geq j \geq 0}, T_0 \right\} \tag{4.7}$$

where operators A_j, B_j, Γ_j and T_j belong to either subspaces V_j or W_j. These operators defined as:

$$A_j = Q_j TQ_j \in W_j \tag{4.8a}$$

$$B_j = Q_j TP_j \in W_j \tag{4.8b}$$

$$\Gamma_j = P_j TQ_j \in V_j \tag{4.8c}$$

$$T_j = P_j TP_j \in V_j \tag{4.8d}$$

and admit the recursive definition

$$T_j = A_{j-1} + B_{j-1} + \Gamma_{j-1} + T_{j-1} \tag{4.9}$$

The wavelet transform recursively represents operators T_j as

$$\begin{pmatrix} A_{j-1} & B_{j-1} \\ \Gamma_{j-1} & T_{j-1} \end{pmatrix} \tag{4.10}$$

which is mapping

$$\begin{pmatrix} A_{j-1} & B_{j-1} \\ \Gamma_{j-1} & T_{j-1} \end{pmatrix} : W_{j-1} \oplus V_{j-1} \to W_{j-1} \oplus V_{j-1} \tag{4.11}$$

The operators A_j, B_j, Γ_j constitute the blocks of NS form. The schematic of the NS form

of matrix is organized in Figure 4.1. In this Figure submatrices $A_j, B_j,$ and Γ_j are non-zero blocks where scale j=1,2,3. The coefficients d^{j-i} and u^{j-i} are the detail and scale coefficients, respectively. The $\bar{g}^{j-i}$ and $\bar{f}^{j-i}$ are the wavelet coefficients of load vector in the NS form.

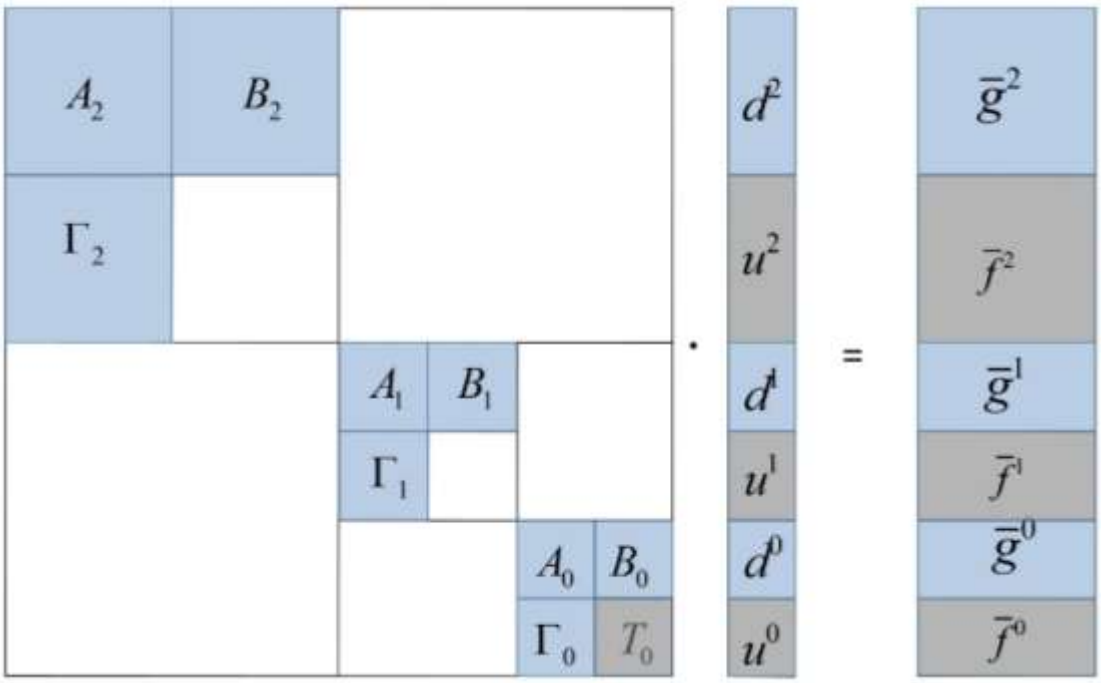

Figure 4.1 Organization of a NS form of the operator *T*

4.2.2 Multiscaling using wavelets

Here, the concept of multiscale analysis using wavelets is directly referred from Section 3.2 of chapter 3. Necessary formulation and finite element discretization of elastic wave propagation has been discussed in subsection 3.2.4 of previous chapter 3. From chapter 3, we know that

$$[\hat{K}][\mathrm{u}]_{s+1} = [\tilde{K}][\mathrm{u}]_s \tag{4.12}$$

If the coefficient vector of $P_j f$ is $u_j = \{u_{j,0}, \ldots, u_{j,v(j)}\}^T$ and coefficient vector of $Q_j f$ is $d_j = \{d_{j,0}, \ldots, d_{j,w(j)}\}^T$ then two levels of resolution (j and $j-1$) in spatial domain can be expressed using wavelet transform as:

$$u_j = [\mathrm{Q}_{j-1} \mid \mathrm{P}_{j-1}] \begin{bmatrix} d_{j-1} \\ \hline u_{j-1} \end{bmatrix} \tag{4.13}$$

After transformation of fine scale u_j, we get coarse scale u_{j-1} which is a kind of average and detail coefficients d_{j-1} which is a kind of difference between fine scale and average coefficients. The insignificant detail coefficients of the smooth region are eliminated to reduce the grid points.

4.2.3 Nonstandard multi-scale decomposition of finite element matrix

Let us consider a continuous wave field $u(x, y)$ and $v(x, y)$ for a source of excitation over 2-D homogeneous medium. The approximation of the continuous wave field on the discrete domain is denoted by u^j and v^j. It represents the discrete wave field that is obtained with a classic time–space finite element method for a sufficiently fine discretization of $V_j \subset \mathbb{R}^2$. The 2-D wavelet transform cascades projections of the discrete wave field over different approximation grids $V_1, V_2, V_3, \ldots\ldots\ldots\ldots, V_j$ of increasing resolution.

In this multi-scale algorithm, we used NS operator proposed by Beylkin (1992). To the best of authors' knowledge, no researcher has used NS operator in wavelet-FEM coupling or wavelet-FDM coupling. It has been proved by Beylkin that NS operator is more efficient than the standard form of operator used by most of the researchers. In this

work, we used NS operator in two-dimensional wavelet finite element coupling technique. The finite element equations for the transient 2D problem, Eq. 4.12, can be expressed in the expanded form as:

$$\begin{bmatrix} \left[k_j^{uu}\right] & \left[k_j^{uv}\right] \\ \left[k_j^{vu}\right] & \left[k_j^{vv}\right] \end{bmatrix} \begin{bmatrix} u_j \\ v_j \end{bmatrix} = \begin{bmatrix} \left[f_j^{u}\right] \\ \left[f_j^{v}\right] \end{bmatrix} \tag{4.14}$$

Using wavelets for forward transformation $T_j = \left[Q_j \mid P_j\right]$, the finest scale is replaced by multiscale as shown in the Figure 4.2. We can apply the wavelet transformation on the field variables of both the directions

$$\begin{bmatrix} \left[\mathrm{T}^T\right] & [0] \\ [0] & \left[\mathrm{T}^T\right] \end{bmatrix} \begin{bmatrix} \left[k_j^{uu}\right] & \left[k_j^{uv}\right] \\ \left[k_j^{vu}\right] & \left[k_j^{vv}\right] \end{bmatrix} \begin{bmatrix} \left[\mathrm{T}\right] & [0] \\ [0] & \left[\mathrm{T}\right] \end{bmatrix} \begin{bmatrix} \left[d_{j-1}\right] \\ \left[u_{j-1}\right] \\ \left[e_{j-1}\right] \\ \left[v_{j-1}\right] \end{bmatrix} = \begin{bmatrix} \left[\mathrm{T}^T\right] & [0] \\ [0] & \left[\mathrm{T}^T\right] \end{bmatrix} \begin{bmatrix} \left[f_j^{u}\right] \\ \left[f_j^{v}\right] \end{bmatrix} \tag{4.15}$$

After rearranging the coefficients, the set of equations can be expressed as:

$$\begin{bmatrix} \begin{bmatrix} \left[k_{j-1}^{dd}\right] & \left[k_{j-1}^{de}\right] \\ \left[k_{j-1}^{ed}\right] & \left[k_{j-1}^{ee}\right] \end{bmatrix} & \begin{bmatrix} \left[k_{j-1}^{du}\right] & \left[k_{j-1}^{dv}\right] \\ \left[k_{j-1}^{eu}\right] & \left[k_{j-1}^{ev}\right] \end{bmatrix} \\ \begin{bmatrix} \left[k_{j-1}^{ud}\right] & \left[k_{j-1}^{ue}\right] \\ \left[k_{j-1}^{vd}\right] & \left[k_{j-1}^{ve}\right] \end{bmatrix} & \begin{bmatrix} \left[k_{j-1}^{uu}\right] & \left[k_{j-1}^{uv}\right] \\ \left[k_{j-1}^{vu}\right] & \left[k_{j-1}^{vv}\right] \end{bmatrix} \end{bmatrix} \begin{bmatrix} \begin{bmatrix} \left[d_{j-1}\right] \\ \left[e_{j-1}\right] \end{bmatrix} \\ \begin{bmatrix} \left[u_{j-1}\right] \\ \left[v_{j-1}\right] \end{bmatrix} \end{bmatrix} = \begin{bmatrix} \begin{bmatrix} \left[g_{j-1}^{u}\right] \\ \left[g_{j-1}^{v}\right] \end{bmatrix} \\ \begin{bmatrix} \left[f_{j-1}^{u}\right] \\ \left[f_{j-1}^{v}\right] \end{bmatrix} \end{bmatrix} \tag{4.16}$$

where d_{j-1} and e_{j-1} are detail coefficients corresponding to the scaling coefficients u_{j-1} and v_{j-1}. The solution can be transformed back in terms of nodal displacement by inverse wavelet transform using Eq. (4.13). These equations are expressed in the NS form after application of next level of wavelet transformation as:

$$\begin{bmatrix} \begin{bmatrix} k_{j-1}^{dd} \end{bmatrix} & \begin{bmatrix} k_{j-1}^{de} \end{bmatrix} & \begin{bmatrix} k_{j-1}^{du} \end{bmatrix} & \begin{bmatrix} k_{j-1}^{dv} \end{bmatrix} & & & & \\ \begin{bmatrix} k_{j-1}^{ed} \end{bmatrix} & \begin{bmatrix} k_{j-1}^{ee} \end{bmatrix} & \begin{bmatrix} k_{j-1}^{eu} \end{bmatrix} & \begin{bmatrix} k_{j-1}^{ev} \end{bmatrix} & & & & \\ \begin{bmatrix} k_{j-1}^{ud} \end{bmatrix} & \begin{bmatrix} k_{j-1}^{ue} \end{bmatrix} & & & & & & \\ \begin{bmatrix} k_{j-1}^{vd} \end{bmatrix} & \begin{bmatrix} k_{j-1}^{ve} \end{bmatrix} & & & & & & \\ & & & & \begin{bmatrix} k_{j-2}^{dd} \end{bmatrix} & \begin{bmatrix} k_{j-2}^{de} \end{bmatrix} & \begin{bmatrix} k_{j-2}^{du} \end{bmatrix} & \begin{bmatrix} k_{j-2}^{dv} \end{bmatrix} \\ & & & & \begin{bmatrix} k_{j-2}^{ed} \end{bmatrix} & \begin{bmatrix} k_{j-2}^{ee} \end{bmatrix} & \begin{bmatrix} k_{j-2}^{eu} \end{bmatrix} & \begin{bmatrix} k_{j-2}^{ev} \end{bmatrix} \\ & & & & \begin{bmatrix} k_{j-2}^{ud} \end{bmatrix} & \begin{bmatrix} k_{j-2}^{ue} \end{bmatrix} & \begin{bmatrix} k_{j-2}^{uu} \end{bmatrix} & \begin{bmatrix} k_{j-2}^{uv} \end{bmatrix} \\ & & & & \begin{bmatrix} k_{j-2}^{vd} \end{bmatrix} & \begin{bmatrix} k_{j-2}^{ve} \end{bmatrix} & \begin{bmatrix} k_{j-2}^{vu} \end{bmatrix} & \begin{bmatrix} k_{j-2}^{vv} \end{bmatrix} \end{bmatrix} \begin{bmatrix} \begin{bmatrix} d_{j-1} \end{bmatrix} \\ \begin{bmatrix} e_{j-1} \end{bmatrix} \\ \begin{bmatrix} u_{j-1} \end{bmatrix} \\ \begin{bmatrix} v_{j-1} \end{bmatrix} \\ \begin{bmatrix} d_{j-2} \end{bmatrix} \\ \begin{bmatrix} e_{j-2} \end{bmatrix} \\ \begin{bmatrix} u_{j-2} \end{bmatrix} \\ \begin{bmatrix} v_{j-2} \end{bmatrix} \end{bmatrix} = \begin{bmatrix} \begin{bmatrix} g_{j-1}^{u} \end{bmatrix} \\ \begin{bmatrix} g_{j-1}^{v} \end{bmatrix} \\ \begin{bmatrix} f_{j-1}^{u} \end{bmatrix} \\ \begin{bmatrix} f_{j-1}^{v} \end{bmatrix} \\ \begin{bmatrix} g_{j-2}^{u} \end{bmatrix} \\ \begin{bmatrix} g_{j-2}^{v} \end{bmatrix} \\ \begin{bmatrix} f_{j-2}^{u} \end{bmatrix} \\ \begin{bmatrix} f_{j-2}^{v} \end{bmatrix} \end{bmatrix} \tag{4.17}$$

The wavelet transform can be continued until a desired low and high frequency component representation is achieved. The well-known standard operator (Eq. (4.15)) can be easily represented in the form of NS operator as shown in Figure 4.1 (Beylkin et al., 1991). The organization of NS form of a matrix for three-level transform is extended in Eq. (4.19), and expressed in the new notations (Gines et al. (1998)) as:

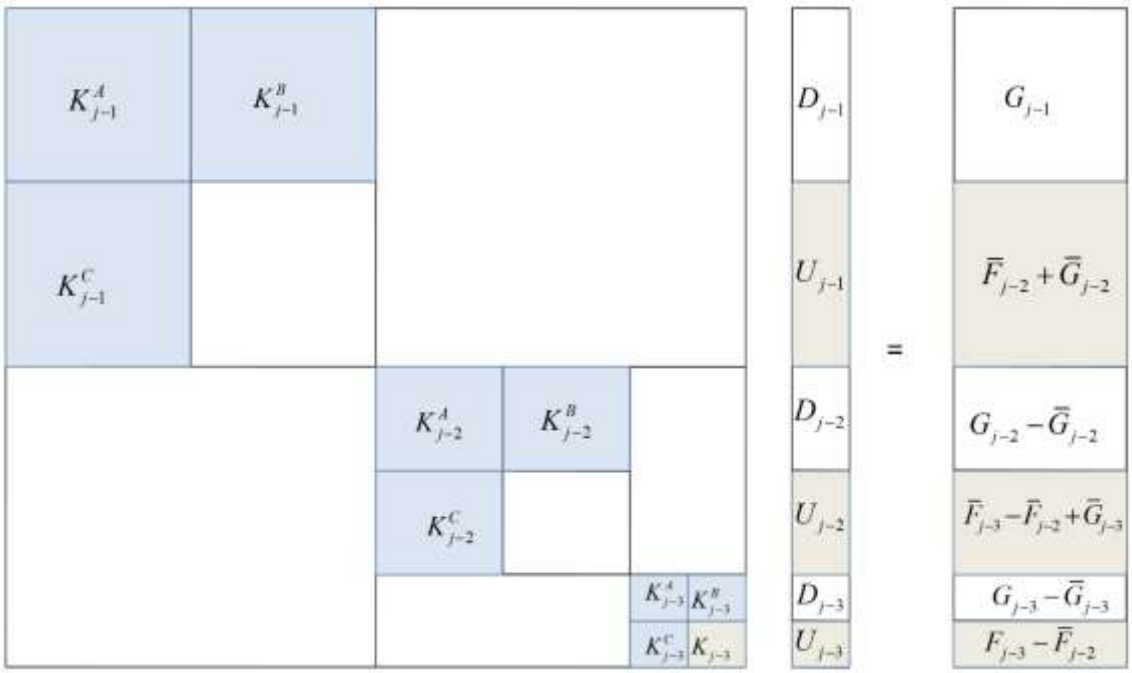

(4.18)

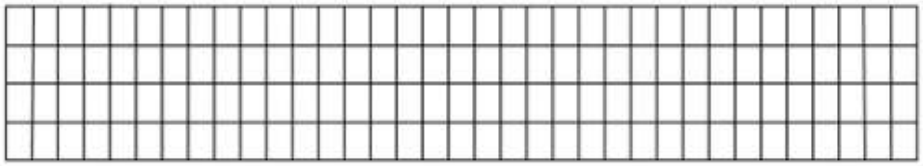

(a) Space V_j

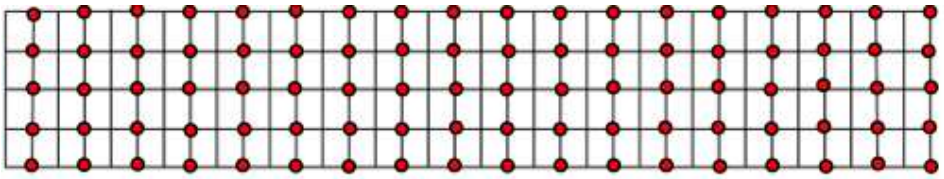

(b) Space $V_{j-1} \oplus W_{j-1}$

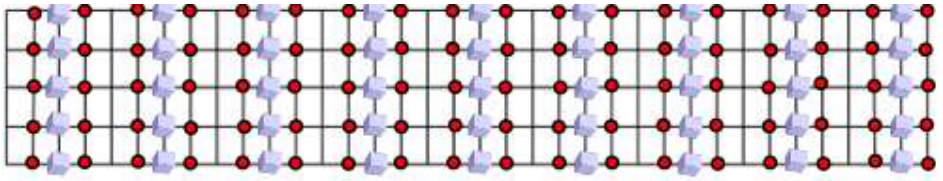

(c) Space $V_{j-2} \oplus W_{j-2} \oplus W_{j-1}$

Figure 4.2. Multi-scale decomposition

where $K_{j-i}^{A} = \begin{bmatrix} [k_{j-i}^{dd}] & [k_{j-i}^{de}] \\ [k_{j-i}^{ed}] & [k_{j-i}^{ee}] \end{bmatrix}, K_{j-i}^{B} = \begin{bmatrix} [k_{j-1}^{du}] & [k_{j-1}^{dv}] \\ [k_{j-1}^{eu}] & [k_{j-1}^{ev}] \end{bmatrix}, K_{j-i}^{C} = \begin{bmatrix} [k_{j-1}^{ud}] & [k_{j-1}^{ue}] \\ [k_{j-1}^{vd}] & [k_{j-1}^{ve}] \end{bmatrix}$ and $K_{j-i} = \begin{bmatrix} [k_{j-i}^{uu}] & [k_{j-i}^{uv}] \\ [k_{j-i}^{vu}] & [k_{j-i}^{vv}] \end{bmatrix}$. The coefficients D_{j-i} and U_{j-i} are the detail and scale coefficients, respectively. The $\bar{G}_{j-i}$ and $\bar{F}_{j-i}$ are the wavelet coefficients of load vector in the nonstandard form and should be converted to standard form by a proper algorithm. In order to solve it, Gines et al. (1998) used LU decomposition. The organization of the LU decomposition is expressed in Eq. ((4.20) -(4.21)) as:

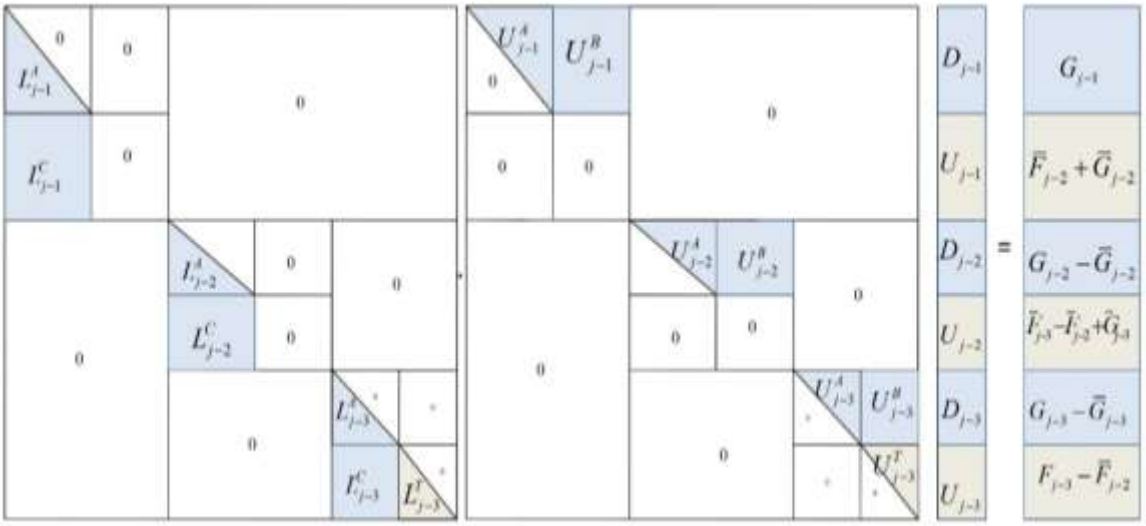

(4.19)

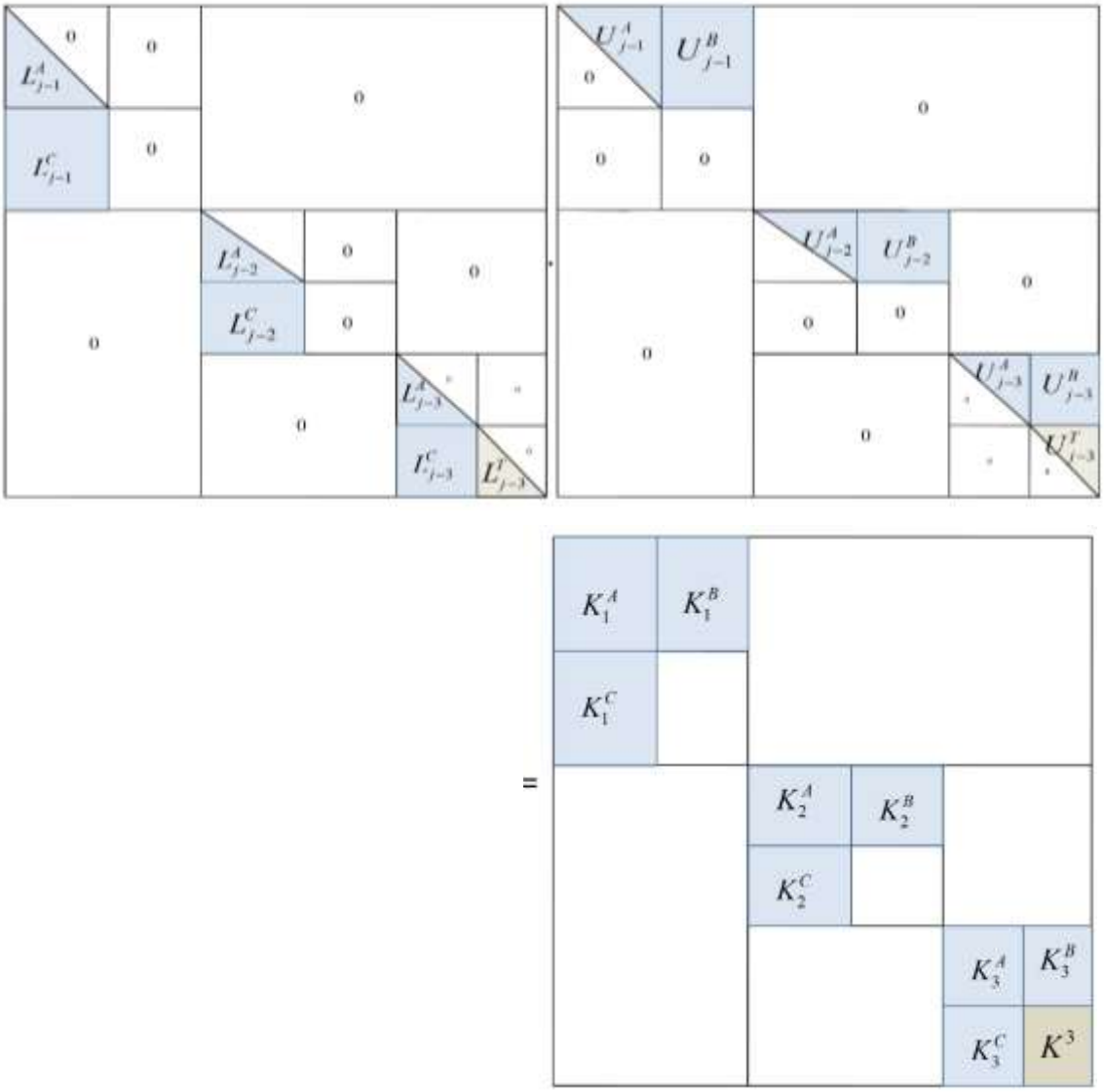

(4.20)

Algorithm 1: LU decomposition of NS operator:

Input: NS form of matrix [A]

Step I: Call LU decomposition algorithm for conversion of lower and upper decomposition of block matrix K_{j-n}^{A} and K_{j-n} from NS form of matrix [A]. Lower block matrix is L_{j-n}^{A}, L_{j-n}^{C} and L_{j-n}^{C}. Upper block matrix is U_{j-n}^{A}, U_{j-n}^{C} and U_{j-n}.

Step II: Computation of elements of block matrix $L_{j-(n-1)}^{C}$ and $U_{j-(n-1)}^{B}$ using $U_{j-(n-1)}^{A}$ and $L_{j-(n-1)}^{A}$ respectively. Where $n = 2,3,\ldots j$.

$$L_{j-(n-1)}^{C} = K_{j-(n-1)}^{C} * \left(U_{j-(n-1)}^{A}\right)^{-1} \qquad \% \quad L_{j-(n-1)}^{A} * \left(U_{j-(n-1)}^{A}\right) = K_{j-(n-1)}^{A}$$

$$U_{j-(n-1)}^{B} = \left(L_{j-(n-1)}^{A}\right)^{-1} * K_{j-(n-1)}^{B}$$

Step III: Convert $[L_{j-(n-1)}^{C}, U_{j-(n-1)}^{B}]$ in standard wavelet transform matrix, which is divided into $\overline{A_2}, \overline{B_2}, \overline{C_2}$ and $\overline{T_2}$.

Step IV: For last scale (final resolution *j*), call LU decomposition algorithm for conversion of lower and upper decomposition of block matrix $[K_{j-(n-1)}^{A} + \overline{A_2}]$ and $[K_{j-(n-1)} + \overline{T_2}]$. After decomposition lower block matrix is L_j^A, L_j^T and upper block matrix is U_j^A, U_j^T respectively.

Step V: Computation of elements of block matrix L_j^C and U_j^B.

$$L_j^C = \left(K_j^C + \overline{C_2}\right) * \left(U_j^A\right)^{-1} \qquad \% \quad L_j^C * U_j^A = K_j^C + \overline{C_2}$$

$U_j^B = \left(L_j^A\right)^{-1} * \left(K_j^B + \overline{B_2}\right)$ % $\left(K_j^B + \overline{B_2}\right) = U_j^B * L_j^A$

Step VI: Find L_j^T and U_j^T using LU decomposition of $[K^j + \overline{T_2} - \left(L_j^C * U_j^B\right)]$

Output: Complete LU decomposition of matrix [A]

The computation of the coefficients is simple and efficient due to LU decomposition of NS form. In this algorithm, submatrices $L_{j-1}^C U_{j-1}^B$, $L_{j-2}^C U_{j-2}^B$ are transformed to next lower scale, therefore, it is necessary to use the algorithm as proposed by Gines et al. (1998) to calculate unknown vector.

In this case of wave propagation, it is observed that wherever dynamic force is smaller than a threshold value $\{f_i\}_s < \varepsilon_f$, the detail coefficients are also smaller than some threshold value $\{d_i^j\}_{s+1} < \varepsilon_d$. Therefore, instead of using $\{d_i^j\}_{s+1}$ for the mask as proposed by other researchers (Vasilyev and Bowman (2000), Bertoluzza (1996)) for their problems, we used dynamic force in the structure $\{f_i\}_s$ to mask V^j. Here $\{f_i\}_s$ is an accurate and cost effective option to locate wave when multiple waves move at different velocities. Let $\wp^0 \cup (\cup_j \Im^j)$ is a set of grid points for the space $V_0 \oplus W_0 \oplus W_1 ... \oplus W_{j-1}$. The grid points associated with $\{f_i\}_s > \varepsilon_f$ create sets $\cup_j M^j$ then the field variable can be expressed as:

$$u^j = \sum_{i \in \wp^0} u_i^0 \varphi_i^0 + \sum_{0 \le j < J} \sum_{i \in M^j} d_i^j \psi_i^j \qquad (4.21)$$

The process to create mask and LU decomposition of NS operator is explained in Algorithm 2 (Cormen et al. 2009).

Algorithm 2: LU decomposition with mask

1. $n \longleftarrow$ *rows*[A]
2. **for** $k \longleftarrow$ 1 **to** n
3. **do** $u_{rr} \longleftarrow a_{kk}$ ▷ The compressed matrix index r corresponds to index k of initial matrix and $r \in \left(\cup_j M^j\right) \cup \wp^0$
4. **for** $i \longleftarrow$ k+1 to n
5. **do** $l_{pr} \longleftarrow a_{ik} / u_{rr}$ ▷ The compressed matrix index p corresponds to index i of initial matrix and $p \in \left(\cup_j M^j\right) \cup \wp^0$
6. $u_{rp} \longleftarrow a_{ki}$
7. **for** $i \longleftarrow$ k +1 to n
8. **do for** $j \longleftarrow$ k +1 to n
9. **do** $a_{ij} \longleftarrow a_{ij} - l_{pr} u_{rq}$ ▷ The compressed matrix index q represent index j of initial matrix and $q \in \left(\cup_j M^j\right) \cup \wp^0$
10. **Return** L and U

4.3 Results and Discussion

The computational cost of simulation of waves with higher harmonics is very high. The objective of the method is to propagate higher harmonics of waves using least number of nodes. To test the wavelet based method, higher harmonics are added in the Lamb wave and propagation of waves is observed. The following actuation function with 400 kHz central frequency driven through a Hanning window is used:

$$F(t) = \begin{cases} A_o \sin(\omega t) * \left(\sin(\frac{\omega t}{10})\right)^2 + \frac{A_o}{10} \sin(10\omega t) * \left(\sin(\omega t)\right)^2, & t < \frac{10\pi}{\omega} \\ 0, & \textit{otherwise} \end{cases} \quad (4.22)$$

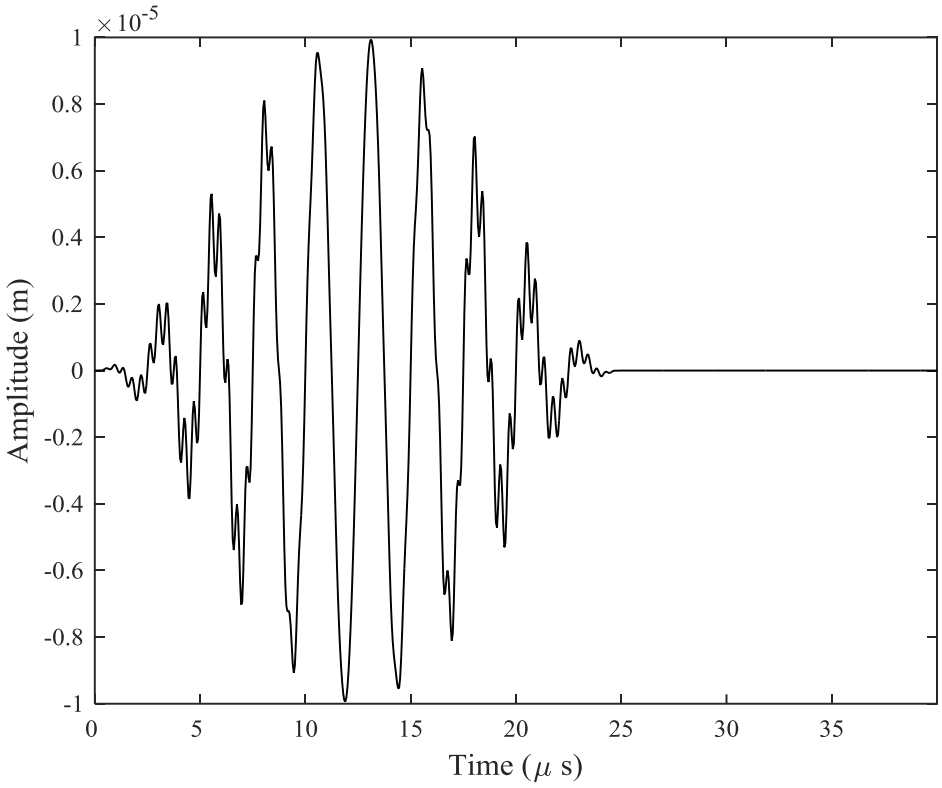

Figure 4.3. Excitation signal for Lamb wave with higher harmonics

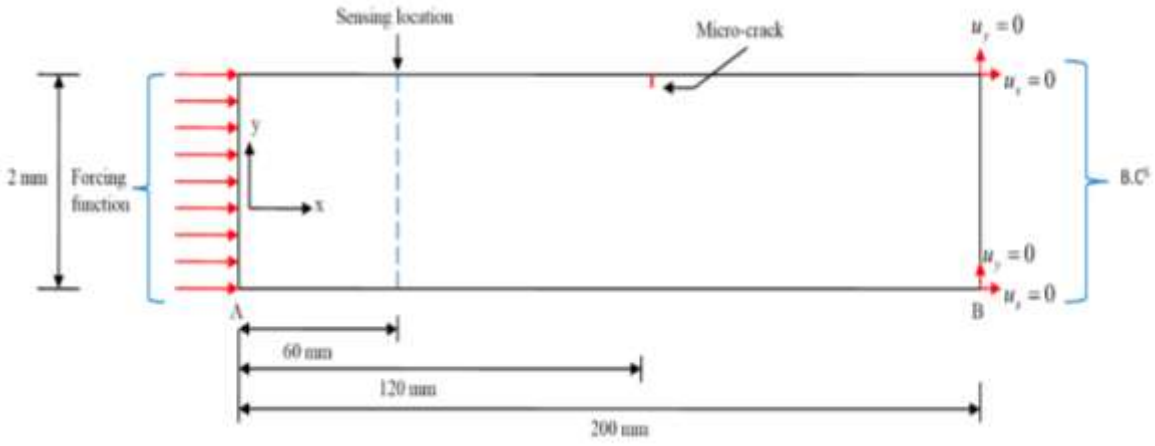

Figure 4.4. Plate geometry, boundary conditions, forcing function and micro crack/ material softening

The excitation signal on a plate with a higher harmonics is shown in Figure 4.3. To provide a limited cycle sinusoidal tone burst, ten cycles Hanning-window excitation signal is applied. An Al plate of 200 mm length and 2 mm thickness is considered in the

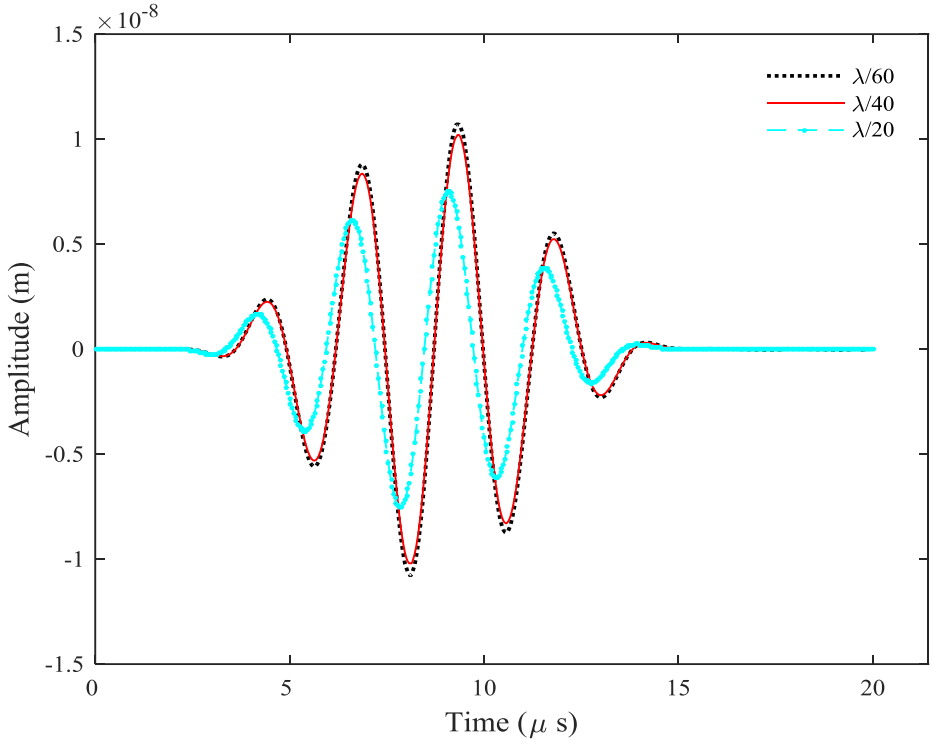

(a) Elements per wavelength

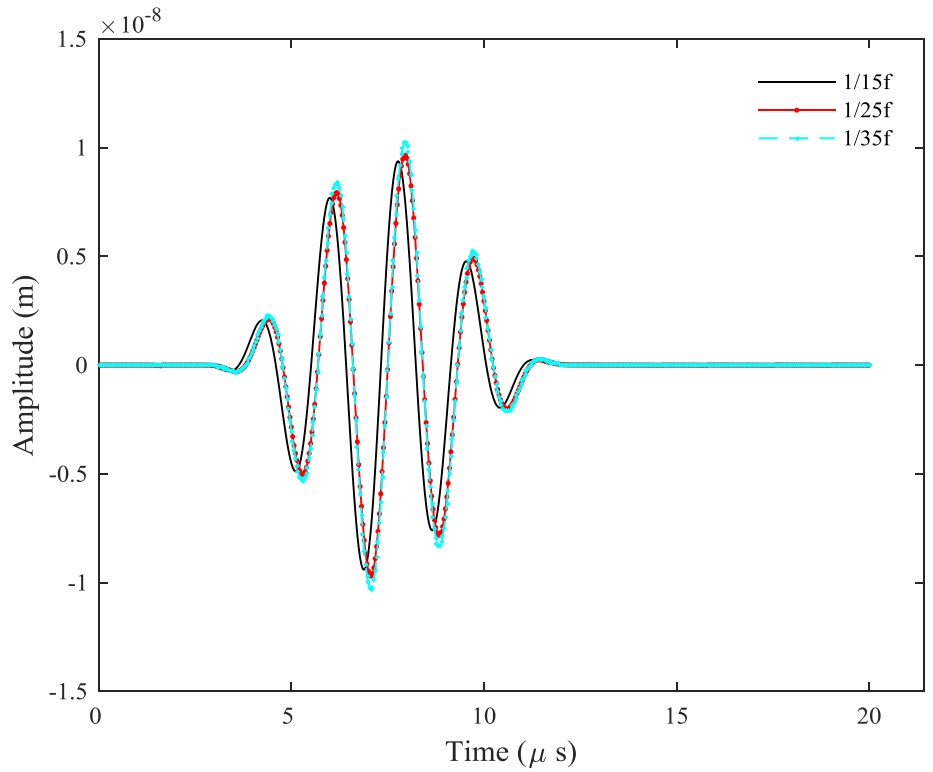

(b) Time steps

Figure 4.5. Convergence of Lamb wave response at healthy plate

analysis. Figure 4.4 shows plate geometry, boundary conditions, displacement u in the direction of wave propagation (x-direction) and v through the thickness (y-direction).The material properties are assumed as Poisson's ratio=0.3, density=2700 Kg/m^3, and Young's modulus E=69 GPa. The Lamb wave in this material has longitudinal velocity C_L = 5299 m/s and transverse velocity C_T= 3135 m/s. The waves are actuated by employing pin forces applied to the left boundary of the plate. The excitation forces are parallel to the longitudinal (propagating) direction. In-phase pin forces are applied to the top and bottom edge nodes of the plate for excitation of fundamental symmetric (S_0) modes, and the anti-symmetric modes are propagated by imposing out-of-phase pin forces. In this thesis, we considered the cases in which the pure S_0 mode is excited.

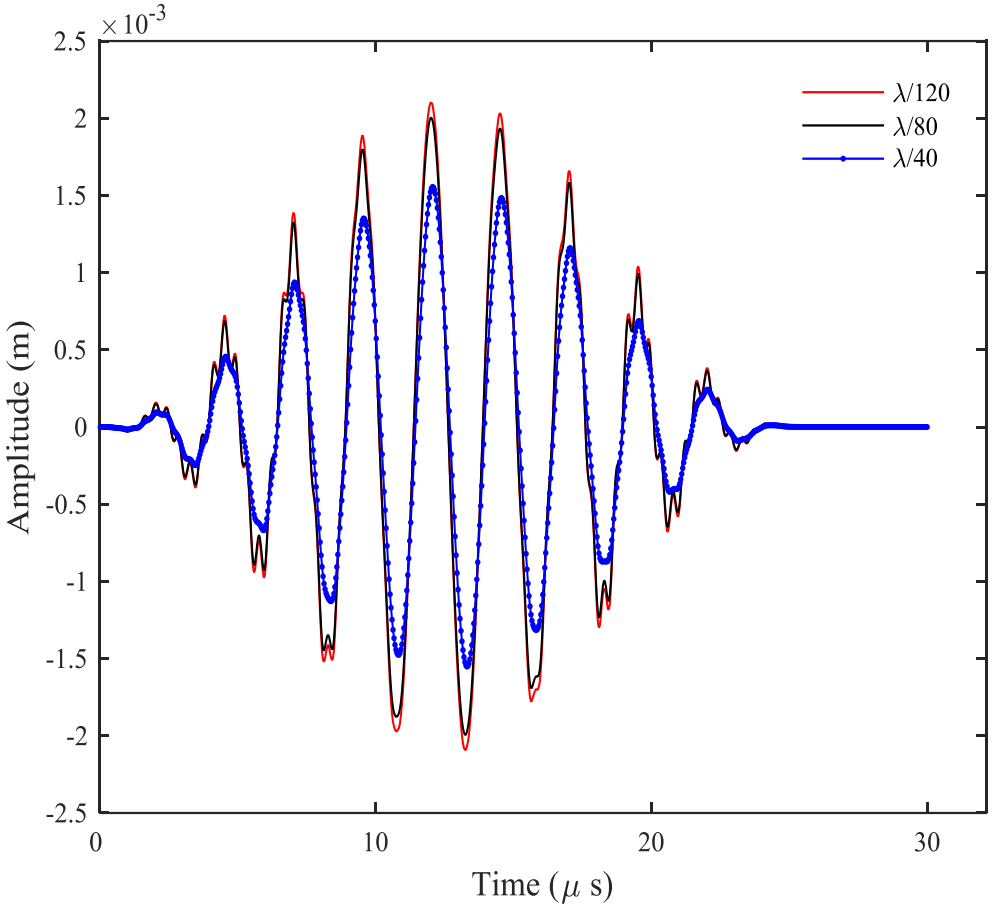

Figure 4.6. Comparison of response of plate for elements per wavelength for higher harmonics

The convergence of elements per wavelength and time steps of linear Lamb wave response at the healthy plate is shown in Figure 4.5(a, b), respectively. It can be seen that 20 elements per wavelength are appropriate for the further simulation of linear Lamb wave (see, Figure 4.5(a)). For time steps, 1/25f is considered for the analysis as shown in Figure 4.5(b). Figure 4.6 depicts the measured nodal displacement response of time-domain signals obtained using FEM simulation of the plate with 40, 80 and 120 elements per wavelength for higher harmonics. It can be observed that higher harmonics are not properly visible in the response of the plate with 40 elements per wavelet. On the other hand, as shown in the same Figure, higher harmonics are visible for 80 elements per wavelength. In this analysis, B-spline and D4 wavelets are used for NS operator.

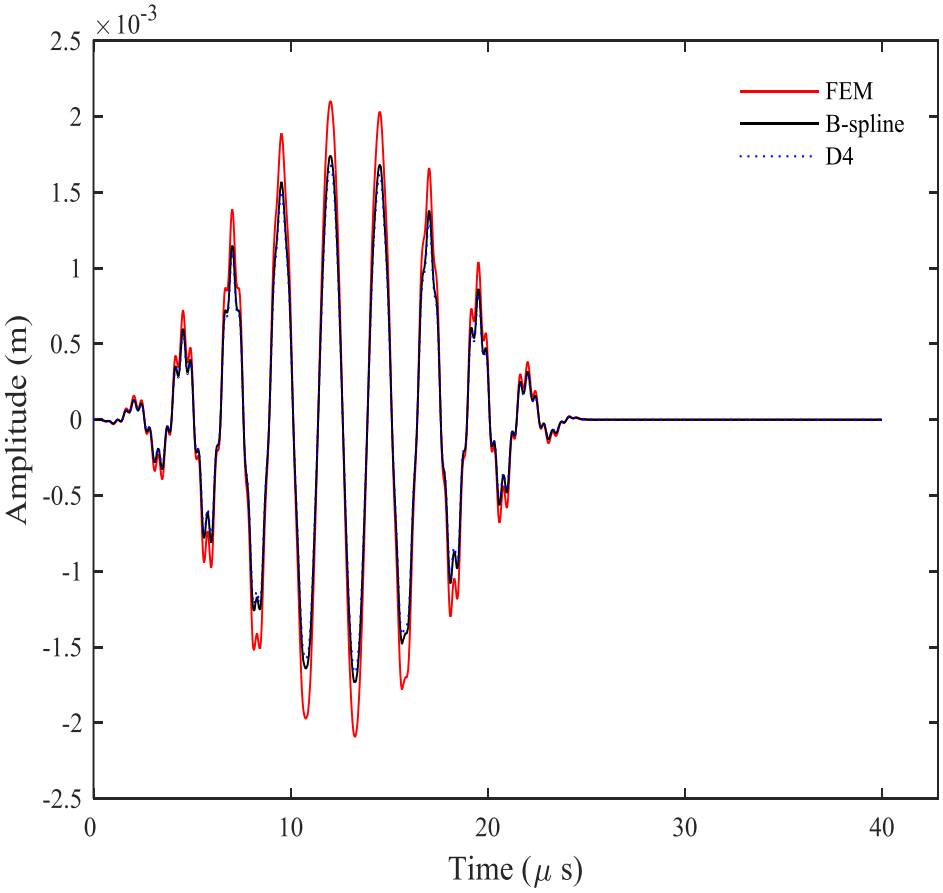

Figure 4.7. Comparison of plate response of higher harmonics at wavelet transform level 3

Nodal displacement response of plate received from B-spline and D4 wavelet Transform at level-3 along with FEM results is demonstrated in Figure 4.7. Wavelet transform at level-3 is utilizing approximately one-eighth of the initial size of FEM matrix. It establishes a good agreement between the conventional finite element and proposed wavelet based method. It can be observed that B-spline wavelet produces response close to FEM results, while there is some deviation in the results of D4 wavelet. These results show some attenuation but wavelets are not eliminating higher frequency components of waves which may be useful in some analysis. Wavelet transform level-4 is also sufficient to propagate higher harmonics but we observed high attenuation. A comparison of B-spline, Haar and Daubechies wavelets of order 4, 6, 8 and 12 is presented at various levels of transforms in Figure 4.8.

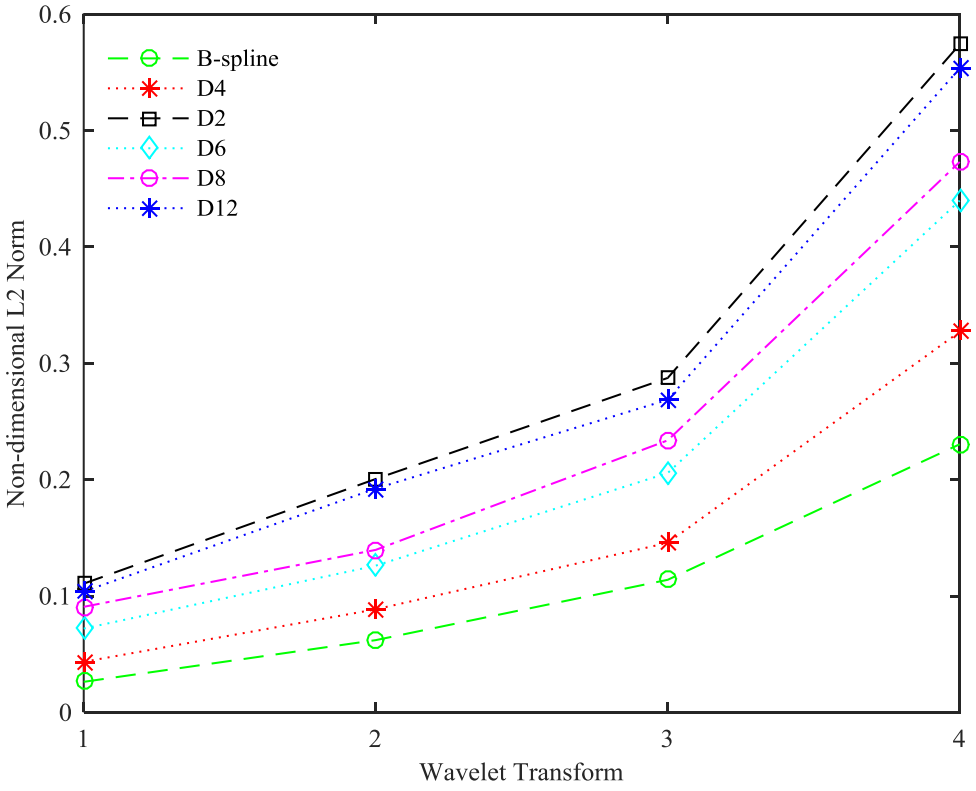

Figure 4.8. Comparison of non-dimentional L_2 norm value for the higher harmonics signal with various wavelet

The difference between the wavelet based methods and FEM solution is measured and showed by the non-dimensional L_2 norm (Shen (2014)).

$$\left\| u_{fem} - u_{wt} \right\| = \sqrt{\sum_{1}^{n} \left(u_{fem} - u_{wt} \right)^2 \Big/ \sum_{1}^{n} u_{wt}^2} \tag{4.23}$$

where n is the length of the time domain signal, and u_{fem} and u_{wt} are the solutions from the FEM method and wavelet based analysis, respectively. It is observed that B-spline is the most suitable wavelet in the present analysis.

For the analysis of plate, fundamental symmetric (S_o) mode centered with excitation frequency 400 kHz of Lamb wave (without higher harmonics) is propagated and the response of healthy plate is shown in Figure 4.9. Figure 4.10 shows FE simulation of reflected wave due to 0.2 mm wide and 0.5 mm deep square notch crack in the plate. The same response can be observed in Figure 4.11 after 3rd level of wavelet transform. At this level, the required number of elements per wavelength is as low as 10 which is the half of the minimum requirement of the element per wavelength in conventional FEM. A comparison of various wavelets response at different levels of the transform for the defective plate is shown in Figure 4.12. It can be observed that for Lamb wave propagation and the same level of compression, B-spline based NS operator is the best.

Prior to the development of cracks due to cyclic loading, nonlinearity due initiation of material softening generate higher harmonics of Lamb wave. Figure 4.13 shows higher harmonics when a soft material (0.1 mm wide and 0.291 mm long) is introduced into the plate in place of the crack. The frequency response of this signal is shown in Figure 4.14. It can be noticed that generation of second harmonics is a good indication of material softening defect.

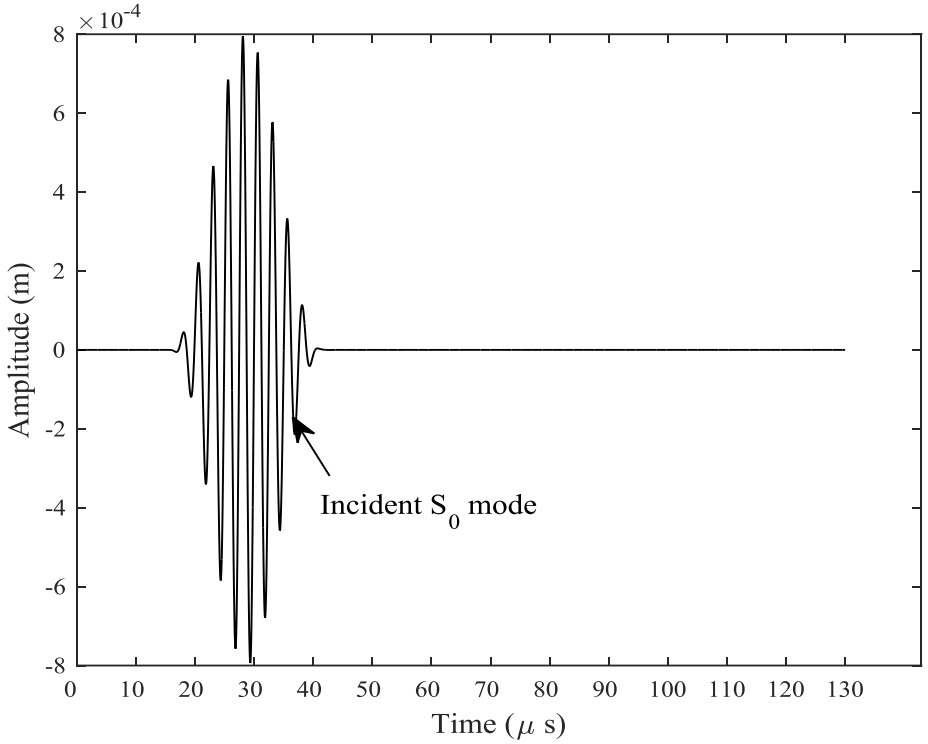

Figure 4.9. Nodal displacement (mm) vs time (microsecond) at sensing location for a healthy plate

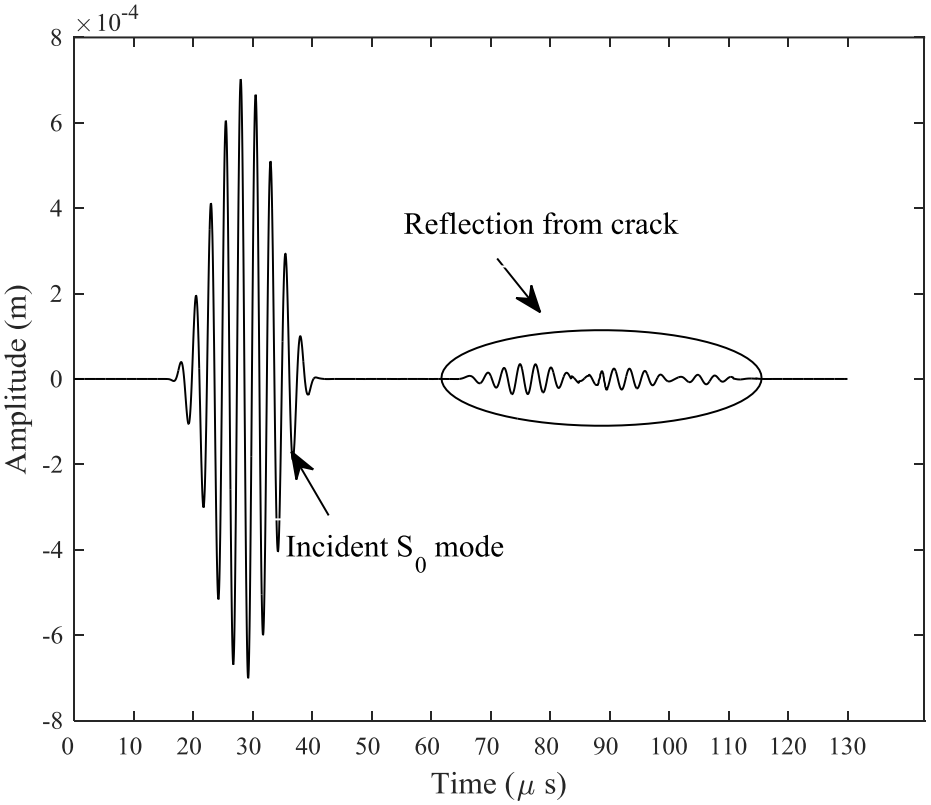

Figure 4.10. Nodal displacement for a plate with crack

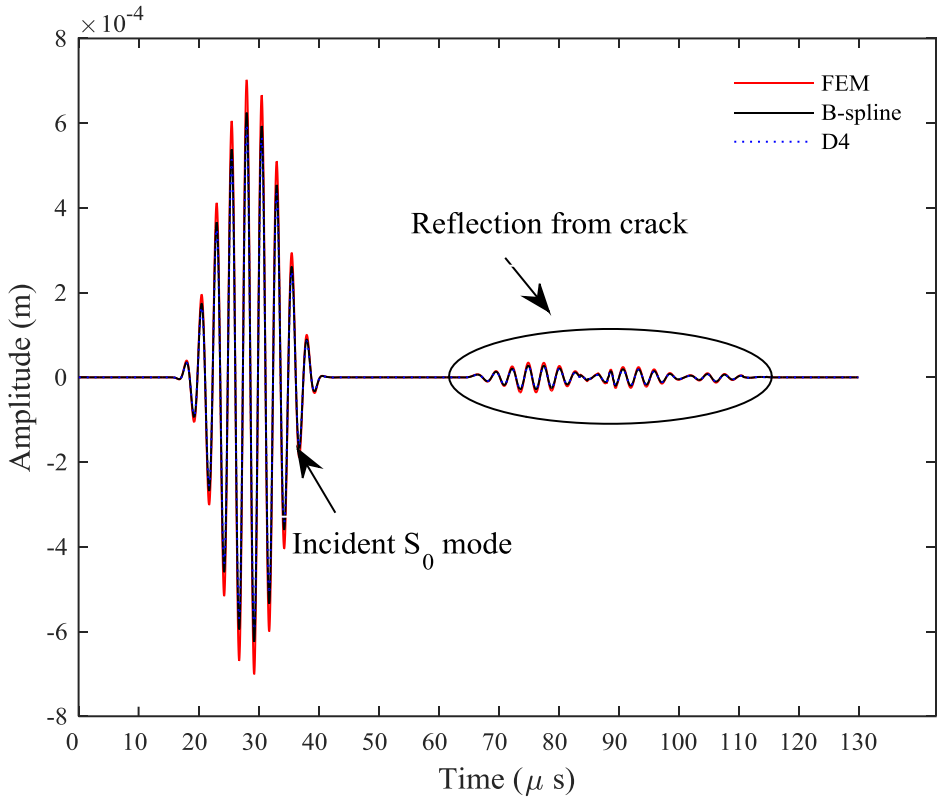

Figure 4.11. Comparison of damage plate response at wavelet transform level 3

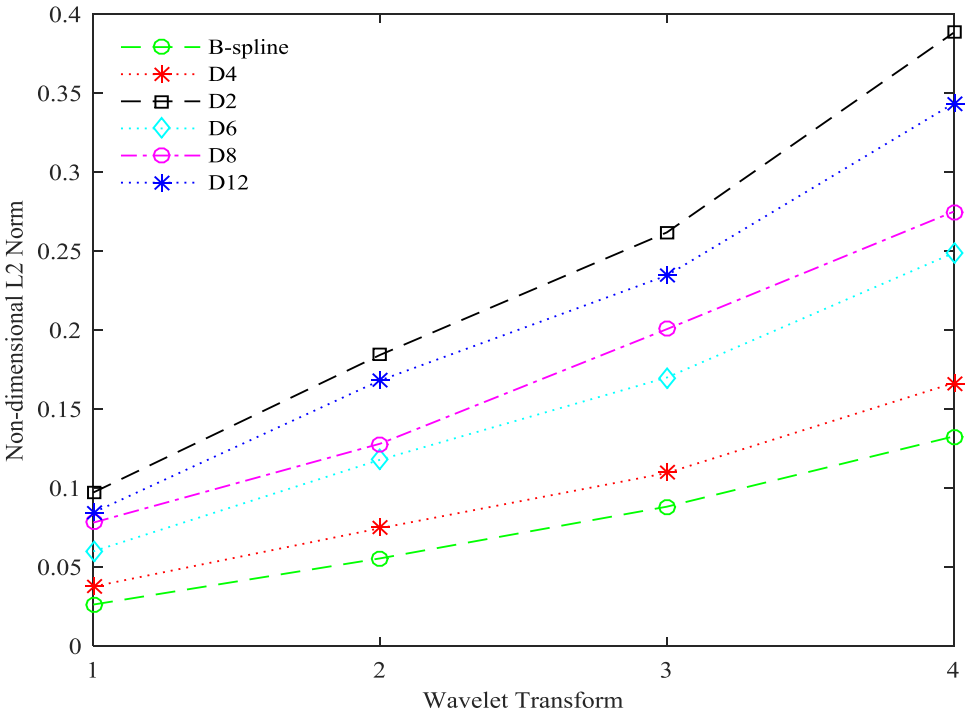

Figure 4.12. Comparison of non-dimentional L_2 norm for various wavelet in damage plate

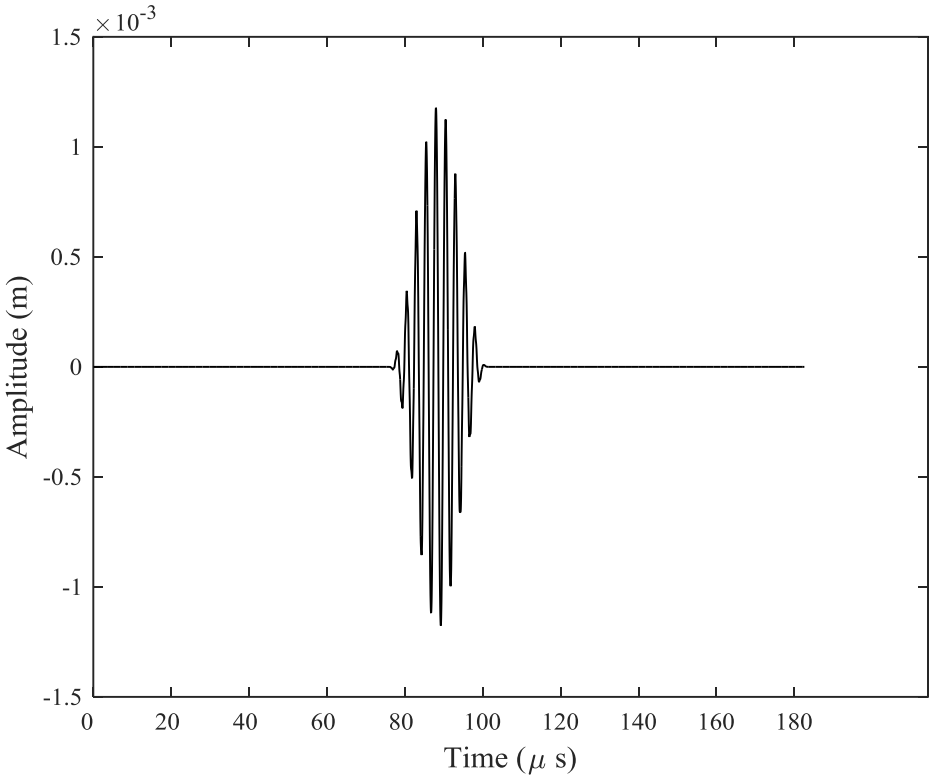

Figure 4.13. The waveform of higher harmonics Lamb waves at the center frequency of 400 kHz

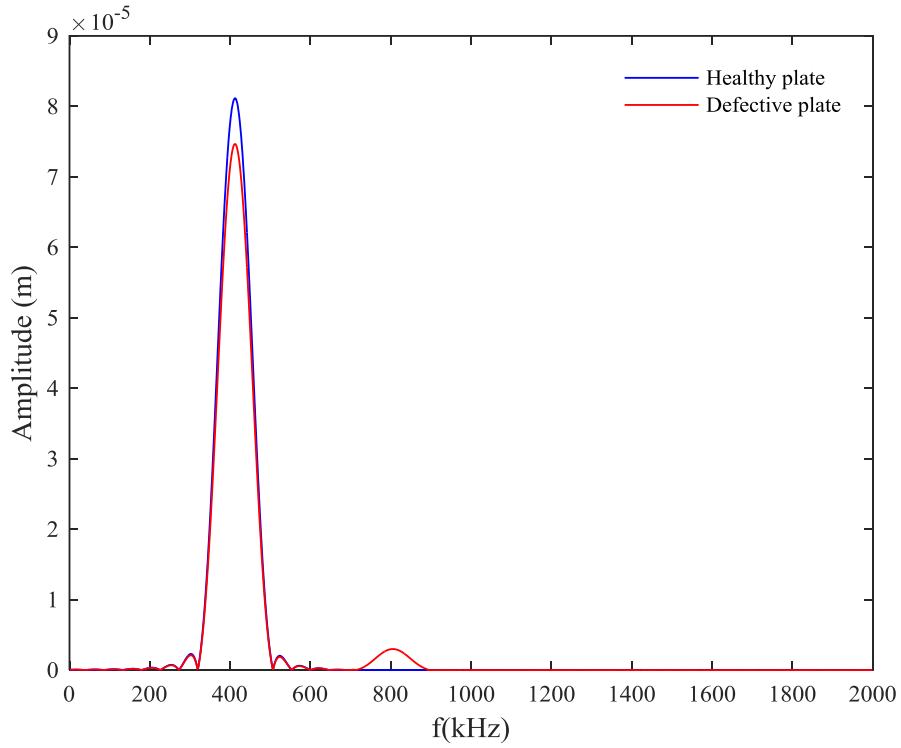

Figure 4.14. The spectrum of higher harmonics Lamb waves at the center frequency of 400 kHz

Table 4.1. Comparison of computational time for the simulation of Lamb wave

Mesh grid	FEM (Time (sec))	Proposed Standard wavelet based method (Time (sec))	Proposed NS wavelet based method (Time (sec))
400×5	97.2589	51.2911	39.8273
800×5	365.4685	180.5208	153.825
1200×5	725.3911	425.3841	385.324
1600×5	1229.361	814.287	765.582
2000×5	2068.4209	1328.326	1216.7
2400×5	3128.3812	2251.755	2097.53
2800×5	out of memory	4987.8338	4713.49

Table 4.1 shows the comparison of execution time (second) for above mentioned Lamb wave problem from all the three methods, namely, FEM, proposed standard wavelet based method and NS wavelet based method. It can be noticed that NS wavelet based technique is significantly reducing the computational time for all the mesh grids and shows the effectiveness of the method. From the table, we can bring into notice of readers that the both proposed methods are very efficient and require lesser execution time compared to conventional FEM.